



Thermophysical properties of liquid UO_2 , ZrO_2 and corium by molecular dynamics and predictive models



Woong Kee Kim ^a, Ji Hoon Shim ^{a, c, **}, Massoud Kaviany ^{a, b, *}

^a Division of Advanced Nuclear Engineering, Pohang University of Science and Technology, Pohang 37673, South Korea

^b Department of Mechanical Engineering, University of Michigan, Ann Arbor, MI 48109-2125, USA

^c Department of Chemistry, Pohang University of Science and Technology, Pohang 37673, South Korea

HIGHLIGHTS

- Comprehensive prediction of the liquid UO_2 , ZrO_2 and corium thermophysical properties by classical molecular dynamics.
- Predicted properties are verified by available experiments and predictive models.
- Correlations for density, specific heat, heat of fusion, compressibility, viscosity, thermal conductivity, and surface tension.

ARTICLE INFO

Article history:

Received 16 September 2016

Received in revised form

14 April 2017

Accepted 20 April 2017

Available online 26 April 2017

Keywords:

Molten (liquid) corium

Molten (liquid) UO_2

Molten (liquid) ZrO_2

Classical molecular dynamics

Density

Specific heat

Heat of fusion

Compressibility

Viscosity

Surface tension

Thermal conductivity

ABSTRACT

Predicting the fate of accident-melted nuclear fuel-cladding requires the understanding of the thermophysical properties which are lacking or have large scatter due to high-temperature experimental challenges. Using equilibrium classical molecular dynamics (MD), we predict the properties of melted UO_2 and ZrO_2 and compare them with the available experimental data and the predictive models. The existing interatomic potential models have been developed mainly for the polymorphic solid phases of these oxides, so they cannot be used to predict all the properties accurately. We compare and decipher the distinctions of those MD predictions using the specific property-related autocorrelation decays. The predicted properties are density, specific heat, heat of fusion, compressibility, viscosity, surface tension, and the molecular and electronic thermal conductivities. After the comparisons, we provide readily usable temperature-dependent correlations (including UO_2 - ZrO_2 compounds, i.e. corium melt).

© 2017 Elsevier B.V. All rights reserved.

1. Introduction

In severe accident of light-water reactors, lava-like molten mixture called corium (compounds of UO_2 , ZrO_2 and Zr) is created due to the radioactive decay and heat of fission. The analysis of such accidents (the fate of the melt), requires accurate corium

thermophysical properties data up to 5000 K [1]. In addition, the initial superheated corium melt, determined from such properties, is key in predicting the fuel-coolant interactions (FCIs) [2] and convection and retention of corium in accident scenarios, e.g. core-melt down corium discharge from reactor pressure vessels and spreading in external core-catcher [3,4]. Due to the very high temperatures, data on molten corium and its constituents are limited, so there are much data scatters and mostly extrapolations (even from solid state) have been used [5]. Here we predict the thermophysical properties of molten UO_2 and ZrO_2 using classical molecular dynamics (MD) simulations (properties of corium are predicted using the mixture theories from UO_2 and ZrO_2 properties). The empirical interatomic potential models are critical in

* Corresponding author. Division of Advanced Nuclear Engineering, Pohang University of Science and Technology, Pohang 37673, South Korea.

** Corresponding author.

E-mail addresses: jhshim@postech.ac.kr (J.H. Shim), kaviany@umich.edu (M. Kaviany).

accurate MD prediction of the properties, and the molten corium constituent oxides, especially UO_2 , have several models developed for the solid phase(s), each tuned to different bulk properties. We compare the predictions and decipher the differences, compare with theoretical predictive models for these properties, and select the most relevant of these models. The predicted properties are density, heat capacity, heat of fusion, compressibility, viscosity, thermal conductivity and surface tension, up to 5000 K and their temperature-dependent useful correlations are provided.

2. Methods

2.1. Interatomic potential models for UO_2 and ZrO_2

We employed the LAMMPS [6] package for the MD simulations to predict the liquid corium properties from atomistic approach. Liquid corium has no microstructure, so such properties are calculated from nanoscale-MD simulating the measured, bulk (macroscopic) properties. The classical MD simulations using interatomic potential models provide robust and efficient prediction of the low symmetry (e.g., liquids) systems [7]. Calculation of properties via MD simulations is governed by the interactions (overlaps) of the atomic orbital. For describing these interactions between atoms, the interatomic force fields are modeled using mathematical relations. The embedded-atom method (EAM) [8] for UO_2 and ZrO_2 is proposed by Cooper et al. (CRG) [9,10], while the traditional Buckingham model [11] for ZrO_2 is additionally introduced by Du et al. (Teter) [12]. The CRG models consider the many-body perturbations in addition to the typical Buckingham-Morse type potentials mainly used for ionic compounds. It models the coordinate-dependent bonding and the violation of the Cauchy relation in metal oxide [13] by the many-body perturbations. The energy of atom i surrounded by atom j is

$$\varphi_i = \frac{1}{2} \sum_j \phi_{\alpha\beta}(r_{ij}) - G_\alpha \left[\sum_j \sigma_\beta(r_{ij}) \right]^{1/2} \quad (1)$$

where α and β are elements of atoms i and j . In Eq. (1), The first term combines the short-range pairwise interaction using the Buckingham [11] and Morse [14] potentials in conjunction with the long-range electrostatic Coulomb interactions, i.e.

$$\phi_{\alpha\beta}(r_{ij}) = A_{\alpha\beta} \exp\left(-\frac{r_{ij}}{\rho_{\alpha\beta}}\right) - \frac{C_{\alpha\beta}}{r_{ij}^6} + D_{\alpha\beta} \left\{ \exp[-2\gamma_{\alpha\beta}(r_{ij} - r_o)] - 2 \exp[-\gamma_{\alpha\beta}(r_{ij} - r_o)] \right\} + \frac{q_\alpha q_\beta}{4\pi\epsilon_0 r_{ij}} \quad (2)$$

The parameters for the short-range pairwise terms and the ionic charges of the Coulombic terms are listed in Table 1.

Table 1

Parameters of the Buckingham and Morse interatomic potentials models in the CRG models [9,10], and the related ionic charges.

	U-U	Zr-Zr	U-O	Zr-O	O-O
$A_{\alpha\beta}$ (eV)	18600	18600	448.779	1147.471	830.283
$\rho_{\alpha\beta}$ (Å)	0.2747	0.23066	0.387758	0.32235	0.352856
$C_{\alpha\beta}$ (eVÅ ⁶)	0.0	0.0	0.0	0.0	3.884372
$D_{\alpha\beta}$ (eV)	–	–	0.66080	1.2269	–
$\gamma_{\alpha\beta}$ (Å ⁻¹)	–	–	2.05815	1.4482	–
r_o (Å ⁻¹)	–	–	2.38051	1.998	–
q_U (e)	+2.2208				
q_{Zr} (e)	+2.2208				
q_O (e)	-1.1104				

The second term in Eq. (1) is a subtle many-body perturbation from the surrounding ions in the EAM formalism and was originally expressed as an approximate function of the electron density functional theory (DFT) for bonding nature of metals [15], with a mathematical analogy to the ionic systems [16]. The G_α is embedding function or energy and σ_β is a set of pairwise functions,

$$\sigma_\beta(r_{ij}) = \left(\frac{n_\beta}{r_{ij}^8}\right) \frac{1}{2} \{1 + \text{erf}[20(r_{ij} - 1.5)]\}. \quad (3)$$

The error function prevents unrealistic dynamics when atoms are very close. The parameters for many-body terms are listed in Table 2.

The Teter potential describes the interaction for ZrO_2 using the short-range Buckingham potential model in conjunction with the long-range Coulombic interaction. The energy of atoms i surrounded by atom j is

$$\varphi_i = \frac{1}{2} \sum_j \phi_{\alpha\beta}(r_{ij}) \quad (4)$$

$$\phi_{\alpha\beta}(r_{ij}) = A_{\alpha\beta} \exp\left(-\frac{r_{ij}}{\rho_{\alpha\beta}}\right) - \frac{C_{\alpha\beta}}{r_{ij}^6} + \frac{q_\alpha q_\beta}{4\pi\epsilon_0 r_{ij}} \quad (5)$$

The parameters for the pairwise term and partial ionic charges are given in Table 3.

In the summation of the system energy, the short-range interactions [the first and second terms in Eq. (5)] are summed with spatial truncation, whereas the long-range interactions [the third term in Eq. (5)] need different approach as elucidated in the next section.

2.2. Coulomb interactions: Particle-Particle-Particle Mesh (PPPM)

Unlike the short-range interatomic potential term, the electrostatic terms [Eq. (6)] remain significant at long distances [17], i.e. the Madelung problem [18], so the Wolf [19] or Ewald [20] methods generally have been employed for accurate summing of the Coulomb term

$$\varphi_i = \frac{1}{2} \sum_j \frac{q_\alpha q_\beta}{4\pi\epsilon_0 r_{ij}} \quad (6)$$

Here we adopted its Particle-Particle-Particle Mesh (PPPM) version of Ewald method [21] which enables a rapid convergence. There is further division into the short-range and long-range terms with the former in the real space and the latter in the reciprocal space (using Fourier transform). Then Eq. (6) becomes

$$\begin{aligned} \varphi_i = & \frac{1}{2} \sum_{j,n} \frac{q_i q_j}{|r_{ij} + nL|} [\text{erfc}(\alpha|r_{ij} + nL|) + \text{erf}(\alpha|r_{ij} + nL|)] - \frac{\alpha q_i^2}{\sqrt{\pi}} \\ & + \frac{2\pi}{3V} q_i r_i \sum_j q_j r_j \\ & + \frac{2\pi}{V} \sum_{k \neq 0} \frac{\exp(-k^2/4\alpha^2)}{k^2} q_i \exp(-ikr_i) \sum_j q_j \exp(-ikr_j). \end{aligned} \quad (7)$$

Table 2

Parameters of the many-body interactions in the CRG models [9,10].

	U	Zr	O
G_α (eV Å ^{1.5})	1.806	1.597	0.690
n_β (Å ⁵)	3450.995	1188.786	106.856

Table 3
Parameters of the Buckingham potentials for the Teter model [12], and related ionic charges in the Coulombic interactions.

	Zr-O	O-O
$A_{\alpha\beta}$ (eV)	7747.1834	2029.2204
$\rho_{\alpha\beta}$ (Å)	0.252623	0.343645
$C_{\alpha\beta}$ (eVÅ ⁶)	93.109	192.58
q_U (e)	+2.4	
q_O (e)	-1.2	

The third term stands for reciprocal space contribution in long-range. Although the cost of conventional Ewald summation results in an order of $N^{3/2}$, where N is the number of atoms in the system, that of the PPPM algorithm is of order $N \log(N)$ with negligible loss of accuracy [22]. Such technique provides more efficient description of the long-range terms (summing energy of the system).

2.3. Equilibrium MD and autocorrelations

2.3.1. Melting procedure

In predicting thermophysical properties of liquid state of corium, it is important to design the initial configuration of liquid state (position of every ion and its interactions). In this work, the UO₂ and ZrO₂ systems are fluorite crystals and are first melted at very high temperatures (around 5000 K) under the *NPT* ensemble for 20 ps with periodic boundary conditions (PBC) and 12000 atoms. The Nose-Hoover thermostat [23,24] and the Parrinello-Rahman barostat [25] are used for controlling temperature and pressure. The liquid state is verified from the atomic structure, the radial distribution function (RDF) and trajectories of atoms. Fig. 1 presents snapshots using OVITO [26] and RDFs for liquid UO₂ and ZrO₂ at 4000 K. No structural coherence is found in both systems and both RDFs show typical liquid behavior.

The atomic trajectories also present the molten state of the system as shown in Fig. 2 for (a) UO₂ (left for U atom and right for O atom), and (b) ZrO₂ (left for Zr atom and right for O atom) for 10 ps. The trajectories show random atomic liquid motion. The cations in both systems move a shorter distance, due to the larger mass. From these results, the liquid atomic structures are verified and are used to conduct equilibrium MD calculations of the liquid properties.

2.3.2. Viscosity calculation: Green-Kubo formula from stress autocorrelation function

For viscosity (μ) calculation in MD, the stress autocorrelation function in the Green-Kubo formulation is employed [27,28].

$$\mu = \frac{V}{k_B T} \int_0^\infty \langle \mathbf{S}(0) \cdot \mathbf{S}(t) \rangle dt, \quad (8)$$

where V , k_B , T , t and \mathbf{S} denote system volume, Boltzmann constant, temperature, time and stress tensor, respectively, and $\langle \dots \rangle$ designates temporal average. The stress tensor is

$$\mathbf{S} = \frac{1}{V} \sum_{i=1}^N \frac{\mathbf{p}_i \mathbf{p}_i}{m_i} + \frac{1}{V} \sum_{i=1}^N \sum_{j>i}^N \mathbf{r}_{ij} \mathbf{F}_{ij}, \quad (9)$$

where \mathbf{p}_i is the momentum vector of atom i , and the vectors \mathbf{r}_{ij} and \mathbf{F}_{ij} are the relative position and force vectors between atom i and j . The decay of the autocorrelation of the xz stress component σ_{xz} is presented for Fig. 3(a). The stress autocorrelation function ($\langle \sigma_{xz}(0) \sigma_{xz}(t) \rangle$) decays over 600 fs for both systems (see Fig. 3(a)).

2.3.3. Thermal conductivity calculation: Green-Kubo heat flux autocorrelation function

In analogy with the viscosity calculations, the molecular conductivity (\mathbf{k}_f) is found from the heat flux autocorrelation function decay using the Green-Kubo formulation [29,30].

$$\mathbf{k}_f = \frac{V}{3k_B T^2} \int_0^\infty \langle \mathbf{q}(0) \cdot \mathbf{q}(t) \rangle dt, \quad (10)$$

where \mathbf{q} is the heat flux vector

$$\mathbf{q} = \frac{1}{V} \frac{d}{dt} \sum_i E_i \mathbf{r}_i = \frac{1}{V} \sum_i E_i \mathbf{u}_i \frac{1}{2V} \sum_i (\mathbf{F}_{ij} \cdot \mathbf{u}_{ij}) \mathbf{r}_{ij}, \quad (11)$$

where \mathbf{u}_i is the velocity vector of atom i .

The decay of auto-correlation function is shown in Fig. 3(b) and occurs over 200 fs for both systems.

2.4. Predictive models for viscosity and thermal conductivity

In addition to the computational MD predictions, the viscosity and molecular thermal conductivity (\mathbf{k}_f) are predicted by models. The Andrade and Bridgman models are employed to the molten UO₂ and ZrO₂, and the corium properties are predicted based on the mixture theories.

2.4.1. Viscosity

The Andrade model [31] explains the temperature dependence of viscosity by temperature agitation interferences with the exchange of momentum [32] and assumes (fluidity or inverse of viscosity) an Arrhenius relation [33].

$$\frac{1}{\mu(T)} = B \exp\left(-\frac{C}{T}\right), \quad (12)$$

where B and C are constants. B is found from the relation for viscosity near the melting temperature where the structure which is not far from the solid phase, but the amplitude of the molecular vibration are different [32]. The relation for the viscosity near the melting temperature (T_m) is

$$\mu(T_m) = A \frac{(mT_m)^{1/2}}{V_A^{2/3}}, \quad (13)$$

where A , m and V_A are constant, atomic mass and volume. The constant C is related to the activation energy (ΔE_a), which is a measure of intermolecular cohesion [34], i.e. $C R_g = \Delta E_a$ [3], where R_g is the gas constant, so the Andrade relation of viscosity is given as [32].

$$\mu(T) = K \frac{(AT_m)^{1/2}}{V_A^{2/3}} \exp\left[\frac{\Delta E_a}{R_g} \left(\frac{1}{T} - \frac{1}{T_m}\right)\right]. \quad (14)$$

For the value of constant K , Andrade proposed [31] 0.161×10^{-6} and Nazare et al. [35] proposed 0.194×10^{-6} . The activation energy (ΔE_a) is estimated as a function of the melting temperature by Gross et al. [36] for metallic systems,

$$\Delta E_a = 1.8 T_m^{1.348} \quad (\text{J/mol}), \quad (15)$$

and Hirai [37],

$$\Delta E_a = 2.65 T_m^{1.348} \quad (\text{J/mol}). \quad (16)$$

The activation energies for liquid UO₂ and ZrO₂ from both formulae are listed in Table 4.

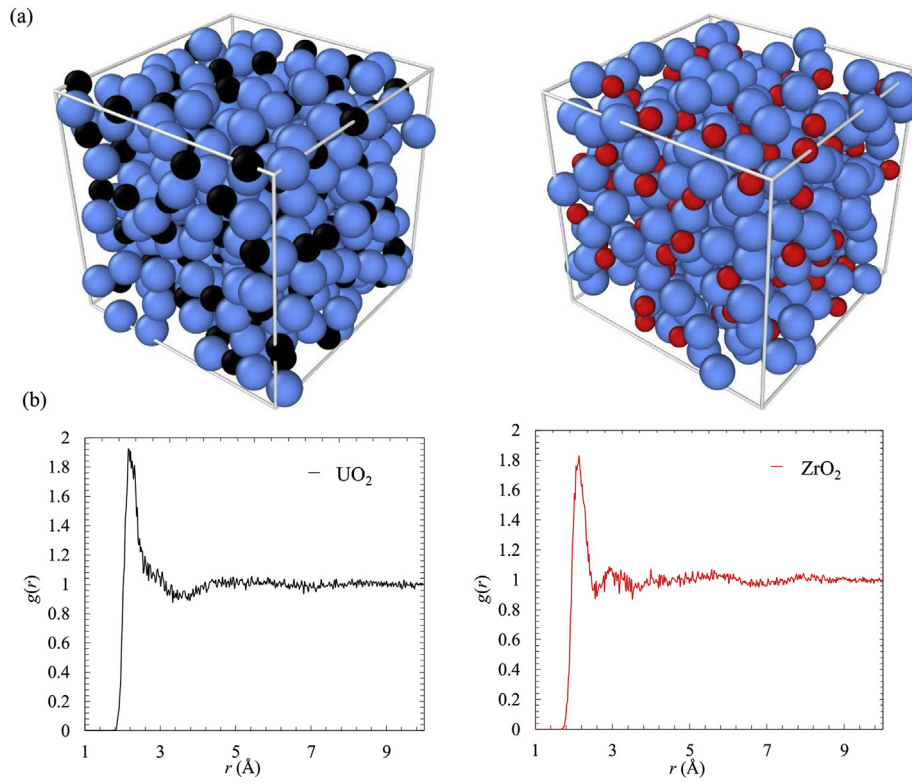


Fig. 1. Atomic structures for liquid (a) UO_2 (left) and ZrO_2 (right) at 4000 K, showing liquid state. Black, red and blue spheres denote U, Zr and O atoms. (b) Radial distribution functions for UO_2 (left) and ZrO_2 (right). The CRG potentials are used for both systems.

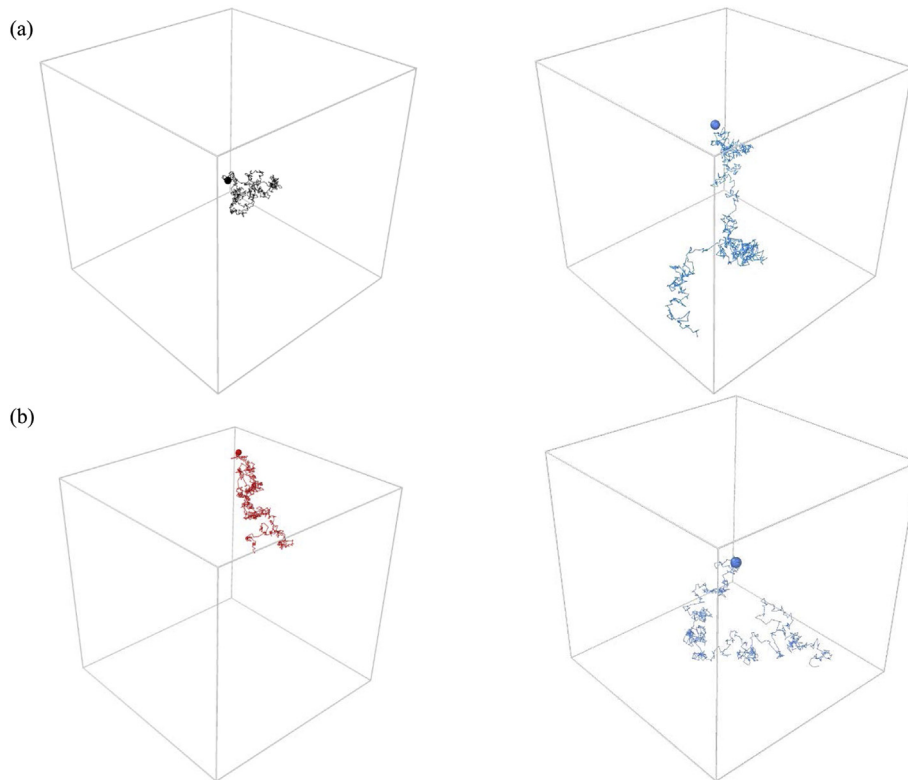


Fig. 2. Atomic trajectories of (a) UO_2 (right: U atom, left: O atom), and (b) ZrO_2 (right: U atom, left: O atom) for 10 ps.

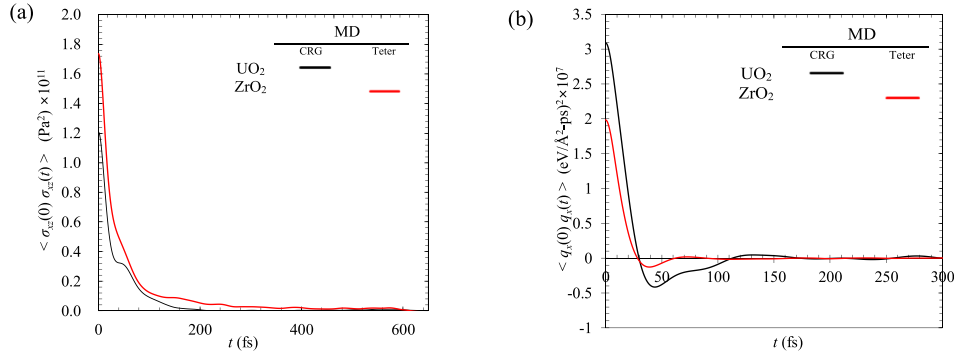


Fig. 3. (a) Decay of the xz-component stress autocorrelation function, for liquid UO₂ and ZrO₂ using the CRG and the Teter potential modes. (b) Decay of the x-component heat flux auto-correlation function, for liquid UO₂ and ZrO₂ using the CRG and the Teter potential models.

In addition, the viscosity of UO₂-ZrO₂ liquid mixture (μ) is modeled by the blending relation under zero excess volume of mixing and Eq. (12) is rearranged for component i with activation energy

$$\frac{1}{\mu_i} \sim \exp\left(-\frac{\Delta E_{a,i}}{R_g T}\right), \quad (17)$$

then the activation energy for binary-mixture system with the molar fraction of component i (x_i) is

$$\Delta E_a = x_1 \Delta E_{a,1} + x_2 \Delta E_{a,2}. \quad (18)$$

Applying this activation energy, we have the viscosity of the mixture

$$\ln \mu = x_1 \ln \mu_1 + x_2 \ln \mu_2. \quad (19)$$

2.4.2. Thermal conductivity

The thermal conductivity of ionic liquid is composed of molecular (k_f) and electronic (k_e). The k_f is predicted by the Bridgman model [38] and assumes that the liquid molecules are in simple cubic arrangements [28], uses the speed of sound [39] ($\langle u_f^2 \rangle = a_s^2$), and a mean free path equal to the molecular spacing $\lambda_f = 3n_f^{-1/3}$, i.e.

$$k_f = \frac{1}{3} \rho_f c_{v,f} \langle u_f^2 \rangle^{1/2} \lambda_f = \rho_f c_{v,f} a_s n_f^{-1/3} = \rho_f c_{v,f} a_s \left(\frac{M}{\rho_f N_A}\right)^{1/3}, \quad (20)$$

where ρ_f , $c_{v,f}$, n_f , M and N_A are density, specific heat, molecule number density, molecular mass and Avogadro number. The Bridgman model is for nonionic liquids, where the molecule moves as a rigid sphere. So, the heat capacity of nonionic liquids is $c_{v,f} = 3R_g/M$ while for ionic liquids UO₂ and ZrO₂, it is taken as $c_{v,f} = 9R_g/M$. The final modified form becomes

$$\begin{aligned} k_f &= \rho_f \frac{9R_g}{M} \left(\frac{c_{p,f}}{c_{v,f}} \frac{\partial \rho_f}{\partial p}\right)^{1/2} \left(\frac{M}{\rho_f N_A}\right)^{1/3} \\ &= \rho_f \frac{9R_g}{M} \left(\frac{c_{p,f}}{c_{v,f}} \frac{1}{\rho_f \kappa_f}\right)^{1/2} \left(\frac{M}{\rho_f N_A}\right)^{1/3} = \frac{9R_g}{N_A^{1/3}} \frac{\rho_f^{1/6}}{M^{2/3}} \left(\frac{c_{p,f}}{c_{v,f}} \frac{1}{\kappa_f}\right)^{1/2}, \end{aligned} \quad (21)$$

Table 4
Activation energy for liquid UO₂ and ZrO₂ from Gross et al. and Hirai.

Activation energy (J/mol)	Gross et al. [36]	Hirai [37]
UO ₂	9.32×10^4	7.31×10^4
ZrO ₂	8.72×10^4	6.87×10^4

where κ_f is the compressibility and $c_{p,f}/c_{v,f} = 1$.

For liquid UO₂ [40]

$$\rho_f(T) = 11.8 - 0.93 \times 10^{-3} T \text{ (g/cm}^3\text{)}, \quad (22)$$

and [41].

$$\kappa_f(T) = \frac{0.05T}{[\rho_f(T)]^3} \text{ (1/MPa} \times 10^{-4}\text{)}. \quad (23)$$

For liquid ZrO₂, the density is [42].

$$\rho(T) = 8.62 - 0.89 \times 10^{-3} T \text{ (g/cm}^3\text{)}. \quad (24)$$

The measure of the isothermal compressibility is reported only at the melting point ($\kappa_{f0} = 0.4231/\text{MPa} \times 10^{-4}$) [42] and the correlation used in Ref. [41] is

$$\kappa_f(T) = \frac{0.03062T}{[\rho_f(T)]^3} \text{ (1/MPa} \times 10^{-4}\text{)}. \quad (25)$$

In addition to molecular thermal conductivity (k_f), the electronic thermal conductivity (k_e) is predicted from the Wiedemann-Franz (W-F) law, relating k_e and the electrical conductivity (σ_e) through the Lorenz number ($N_L = 2.44 \times 10^{-8}$ W-Ω/K²) [35].

$$k_e = \sigma_e N_L T \quad (26)$$

and [43].

$$\sigma_e = n_{e,c} e c \mu_e, \quad (27)$$

where $n_{e,c}$ is the free carrier (electron) density, e_c is the electron charge and μ_e is the carrier mobility. The intrinsic conduction-band electron density ($n_{e,c}$) for nondegenerate state is [30].

$$n_{e,c} = \frac{2(2\pi m_{e,e} k_B T)^{3/2}}{h_p^3} \exp\left(-\frac{\Delta E_{e,g}}{2k_B T}\right), \quad (28)$$

where $m_{e,e}$ is the electron effective mass, $\Delta E_{e,g}$ is the bandgap and h_p is the Planck constant. Here we use the simplified relation [43] with considering temperature dependence of mobility ($\mu_e \propto T^{-3/2}$),

$$\sigma_e = \sigma_0 \exp\left(-\frac{\Delta E_{e,g}}{2k_B T}\right), \quad (29)$$

where σ_0 is the constant pre-exponential factor. So, the electronic thermal conductivity becomes

$$k_e = L\sigma_0 T \exp\left(-\frac{\Delta E_{e.g}}{2k_B T}\right). \quad (30)$$

For the mixture thermal conductivity (k), the empirical relation by Filippov and Novoselova [44], [45] is employed with total thermal conductivity of component i (k_i),

$$k(T) = x_1 k_1(T) + x_2 k_2(T) - 0.72 x_1 x_2 |k_1(T) - k_2(T)|, \quad (31)$$

where $k = k_f + k_e$.

2.5. Liquid surface tension from equilibrium MD

The surface tension is the key properties which significantly influence on the morphology of corium melt and equilibrium MD simulations are used under a liquid-vapor interface. After atomic structure is fully melted under PBC in Section 3.1, the system boundary normal to z -direction is changed to a free surface at the target temperature, and the liquid-vapor interface is created as shown in Fig. 4(a). After steady state reached, the tangential pressure (stress) at the interface is different from the normal pressure and the surface tension σ is enticed from the difference at the surface as [46].

$$\sigma = \int_{-\infty}^{\infty} [p_n(z) - p_t(z)]/2 \, dz, \quad (32)$$

where $p_n(z)$ and $p_t(z)$ are normal and tangential pressure tensor components depending on the coordinate z . Since the integral is over the liquid-vapor slab having two free surfaces, the pressure distribution is divided by 2 in Eq. (32). Normal and tangential pressure components along the z -direction are

$$p_n(z) = p_{zz}(z) \text{ and } p_t(z) = \frac{p_{xx}(z) + p_{yy}(z)}{2}. \quad (33)$$

The expression for the pressure (stress) tensor in virial form [46] is

$$p_{ab} = \frac{1}{V} \sum_i r_{ia} F_{ib}, \quad (34)$$

where i is atom index and ab is component of the tensor, r and F are components of location and force vectors of i , respectively. In the MD simulations, the distribution of the pressure difference [integrant of Eq. (32)] is obtained along the z -direction [Fig. 4(b)] and averaged over 50 ps (The Wolf method [19] is employed for the

charge summation as a sufficiently accurate condition, since the PPPM version of the Ewald method is only applied for the PBC).

3. Results and discussion

3.1. Density

The MD predicted the temperature-dependent densities of liquid UO_2 and ZrO_2 , using the CRG potential models, as shown in Fig. 5(a), from near the melting point (3200 K for UO_2 and 3000 K for ZrO_2) up to 5000 K. These are compared with the reported correlations based on experiments [Eq. (22) for UO_2 and Eq. (24) for ZrO_2]. The predicted UO_2 density is well matched with the experimental results on the temperature range. The predicted ZrO_2 density is reasonable compared to experiments. We also predicted the ZrO_2 density using the Teter potential models, as shown in Fig. 5(b) and it underpredicts the density compared to the result of the CRG models and experiments.

The density of corium mixture (ρ) is estimated from the molar fraction of component i (x_i) based on the assumption of ideally mixture (without excess volume creation), presented in Table 5. This is a reasonable assumption, since for example liquid SiO_2 has excessive volume of 1% [47].

3.2. Heat capacity

The temperature-dependent MD predicted the heat capacity of liquid UO_2 and ZrO_2 , using the total energy dependence on the temperature up to 5000 K are compared with reported experimental result [41,42,48–50] in Fig. 6(a). The MD predictions present good agreement with the experiments. The UO_2 experimental result have a large scatter, and the MD results are in the middle of the reported values. The heat capacity for ZrO_2 is nearly constant as 815 J/kg-K. A small decrease of ZrO_2 heat capacity is due to the thermal expansion and the decrease in the potential energy. For ZrO_2 , the heat capacity evaluated by the Teter potential models is also compared with the results from the CRG potential models and the experiments as shown in Fig. 6(b). The Teter models give similar heat capacity compared with the CRG models and the experiments. As will be shown later, this does not hold for other properties. The heat capacity of mixture state is predicted from interpolation between heat capacities of pure UO_2 and ZrO_2 , depending on the mass fraction (Table 5.)

3.3. Heat of fusion

The heat of fusion is of importance in predicting and simulation

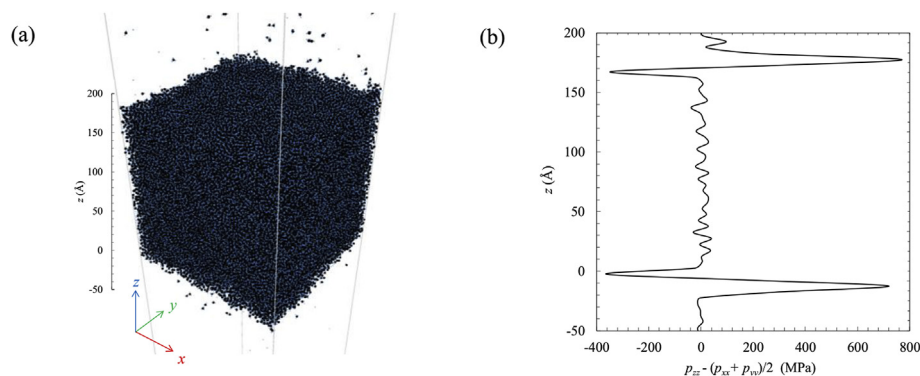


Fig. 4. (a) Perspective view of UO_2 liquid-vapor interfaces (top and bottom) showing the vapor phase, at $T = 3500$ K and using the CRG potential model. (b) Spatial distribution of pressure integrant of surface tension relation for liquid UO_2 using the CRG potential models. The peaks are at the liquid-vapor interfaces.

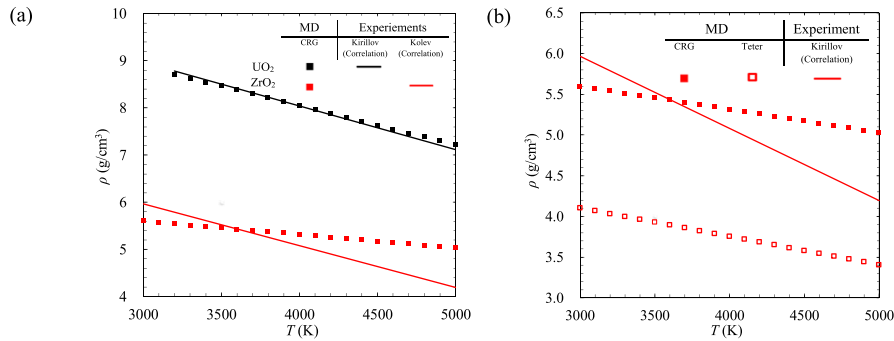


Fig. 5. (a) Variations of MD predicted liquid UO_2 and ZrO_2 density with temperature, using the CRG potential models and comparison with experiments. (b) Variations of MD predicted liquid ZrO_2 density with temperature, using two different sets of interatomic potential models, and comparison with experiment.

of the fate of the corium and its eventual solidification.

The heat (enthalpy) of fusion of UO_2 and ZrO_2 is predicted with the equilibrium MD simulations using the CRG and Teter models, as change of enthalpy between the liquid and solid phases. Specifically, the MD enthalpies of the initial solid and liquid phases are calculated first under the NPT ensemble by varying the system temperature near the melting point (for UO_2 , the melting temperature is predicted with the CRG models and is between 3000 and 3100 K [9]).

The predicted heat of fusion for UO_2 by CRG models is $\Delta h_{sl} = 218$ kJ/kg and in good agreement with measured values from experiment of for 259 kJ/kg [51].

For ZrO_2 the MD predictions of the heat of fusion by both potential models give 260 kJ/kg (the CRG models) and 404 kJ/kg (the Teter models). The experimental result is 706 kJ/kg [52]. To examine these further, we use the predictive model of the heat of fusion by Garai [51] which considers the phase transition energy to overcome the viscous resistance for departing from the symmetric atomic arrangement in the solid, assuming atoms move with the thermal speed ($\langle u_f \rangle = (k_B T_m / M)^{1/2}$), then upon melting this energy (heat of fusion) is

$$\Delta h_{sl} = \frac{1}{(n+1)^2} \frac{V_m}{d} \mu \langle u_f \rangle, \quad (35)$$

where n is the number of coupled atoms between a pair of atoms moving with speed $\langle u_f \rangle$, V_m is molar volume and d is atomic diameter. The viscosity at the melting point is found using Eq. (13). For $n = 1$ and d as the cube root of the averaged molecular volume, the heat of fusion for UO_2 is 173 and for ZrO_2 is 212 kJ/kg.

Therefore, when considering the predictive model results, the

above CRG potential MD predicted value of 218 kJ/kg for UO_2 and 260 kJ/kg for ZrO_2 appear reasonable. While, the experimental result for ZrO_2 appears to be rather high, considering that the viscosity and melting temperatures of ZrO_2 and UO_2 are rather close (i.e. we do not expect their heat of fusion to be vastly different, opposite to the trend in the experimental results). Heat of fusion of mixture is estimated from interpolation between pure UO_2 and ZrO_2 , depending on mass fraction (Table 5).

3.4. Isothermal compressibility

The temperature-dependent isothermal compressibility of liquid UO_2 and ZrO_2 is predicted by the equilibrium MD simulations using the CRG and the Teter models. The volume fluctuation theory [39] is used under the NPT ensemble

$$\langle \delta V^2 \rangle_{NPT} = \kappa_f V k_B T, \quad (36)$$

The results are shown in Fig. 7(a). The predictions are compared with the experiments [43,44,48,52]. The experimental value of ZrO_2 (Kolev) is extrapolated using the fitting relation [Eq. (25)] proposed by Brietung and Reil [41]. The other correlation on ZrO_2 (Kolev) is derived from a constant sound velocity (u_a) [42].

$$\kappa_f = \frac{1}{\rho(T) u_a^2}. \quad (37)$$

In Fig. 7(a), the predicted UO_2 compressibility is in middle of experimental scatter. The predicted ZrO_2 compressibility allows for guidance in the vastly scattered experiments/correlations. We also calculate the compressibility using with the CRG models for ZrO_2 and they are compared with the results of Teter models and

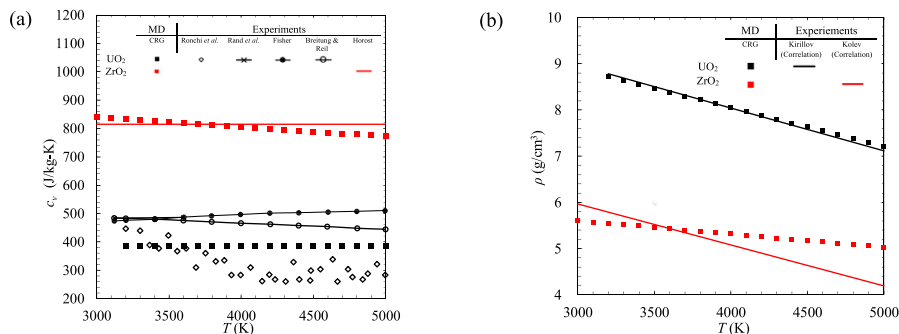


Fig. 6. (a) Variations of MD predicted of liquid UO_2 and ZrO_2 specific heat at constant volume with temperature, and comparison with experimental results. (b) Variations of MD predicted liquid ZrO_2 heat capacity with temperature, using two different sets of interatomic potential models, and comparison with experiment.

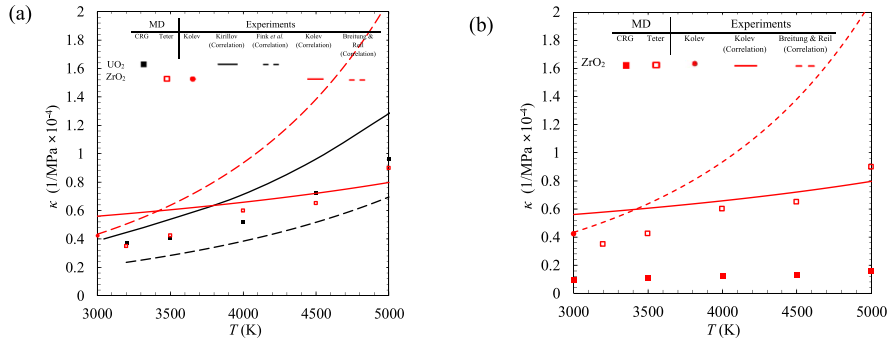


Fig. 7. (a) Variations of MD predicted liquid UO_2 and ZrO_2 compressibility with temperature, and comparison with experiments. (b) Variations of MD predicted liquid ZrO_2 compressibility with temperature, using two different sets of interatomic potential models, and comparison with experiments.

experiments as shown in Fig. 7(b). The Teter models well predict the compressibility of liquid ZrO_2 compared with correlation based measurement near the melting temperature. The CRG models underpredict and show weak temperature dependence in contrast to the correlations.

The formula of the mixture compressibility is give in Table 5 same as density of mixture.

3.5. Viscosity

Based on the Green-Kubo formulation, the viscosity of liquid UO_2 and ZrO_2 are predicted as a function of temperature and shown in Fig. 8(a). The simulation-size effect was examined and found to be negligible (the viscosity calculations using the Green-Kubo formulation). The predicted results present good agreement with the experiments [35,49,50] and the predictive Andrade model [31]. In Andrade model of Eq. (14), $K = 0.194 \times 10^{-6}$ from Nazare et al. [35] and the activation energy is from Hirai et al. [37], so for UO_2 and ZrO_2 we have

$$\mu(T) = 0.520 e^{8.26 \times 10^3 / T}, \quad \mu(T) = 0.351 e^{8.79 \times 10^3 / T} \quad (38)$$

$$\mu(T) = 0.320 e^{8.79 \times 10^3 / T}, \quad \mu(T) = 0.312 e^{8.26 \times 10^3 / T} \quad (39)$$

The predicted UO_2 viscosity falls in the middle of the dispersed experimental results. The predicted ZrO_2 viscosity is larger compared to the experimental results at the melting temperature. Despite the absence of pertinent experimental results, both predicted viscosities are in good agreement with the Andrade models. The predicted ZrO_2 viscosity using both the CRG and Teter models is also provided in Fig. 8(b), and overpredicts the experiments.

Fig. 8(c) shows the temperature dependence of the viscosity of liquid UO_2 - ZrO_2 mixture (corium) for various compositions. The blending equation [Eq. (19)] and the Andrade models for UO_2 and ZrO_2 [Eqs. (37) and (38)] are used for the composition from $(\text{UO}_2)_{0.8}(\text{ZrO}_2)_{0.2}$ to $(\text{UO}_2)_{0.2}(\text{ZrO}_2)_{0.8}$. The viscosity is evaluated above 3200 K (melting temperature of UO_2). The viscosity of UO_2 and ZrO_2 are very close.

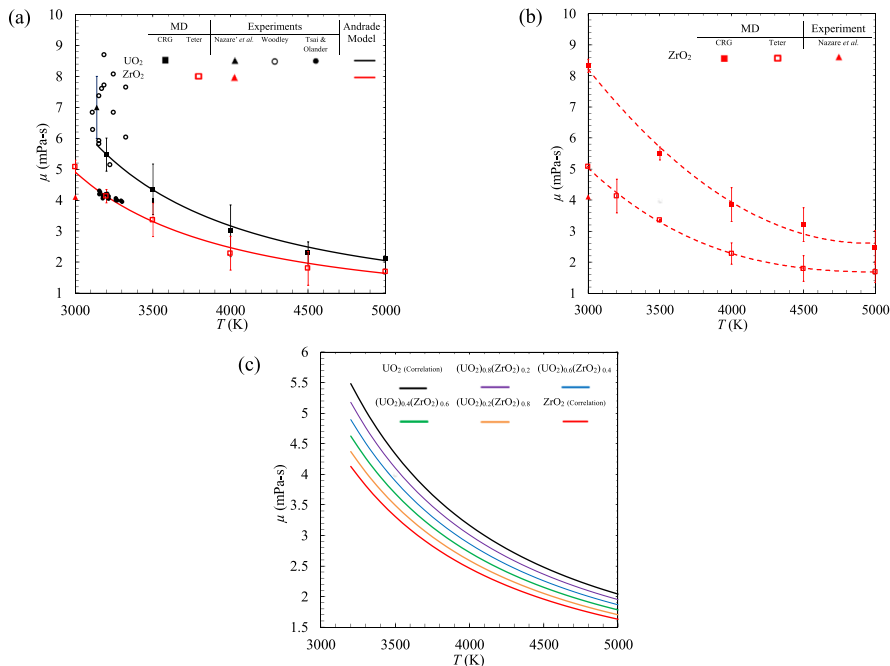


Fig. 8. (a) Variations of MD predicted liquid UO_2 and ZrO_2 viscosity with temperature, and comparison with experiments and with predictive model. (b) Variations of MD predicted liquid ZrO_2 viscosity with temperature, using two different sets of interatomic potential models, and comparison with experiments. (c) Variations of liquid UO_2 - ZrO_2 mixture (corium) viscosity with temperature, for several compositions.

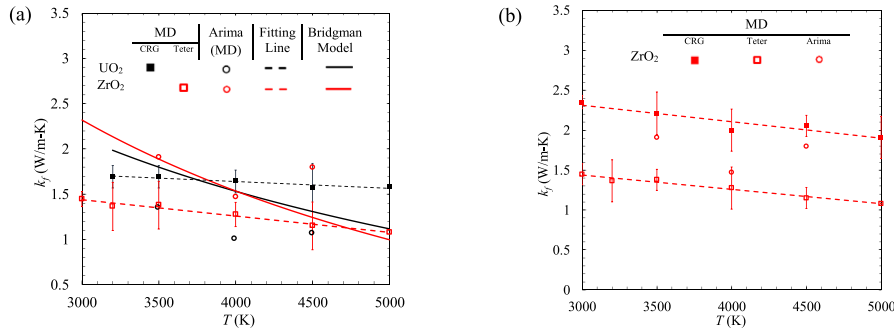


Fig. 9. (a) Variations of MD predicted liquid UO_2 and ZrO_2 thermal conductivity with temperature, and comparison with available MD results and with predictive model. (b) Variations of MD predicted liquid ZrO_2 thermal conductivity with temperature, using two different potential models, and comparison with available MD results (Arima [53]).

3.6. Thermal conductivity

The thermal conductivity of ionic liquids is obtained by the molecular k_f and the electronic k_e contributions respectively. The k_f is predicted by the MD simulations and the Bridgman model, while the k_e is predicted by the Widemann-Franz law. The predicted k_f of liquid UO_2 and ZrO_2 as a function of temperature are shown in Fig. 9(a). The simulation size effect check showed negligible change. The CRG potential is used for UO_2 and the Teter potential is used for ZrO_2 . The prediction are compared with other reported MD predictions by Arima [54] and the Bridgman model. Our MD predicted UO_2 thermal conductivity shows temperature independence, while the Bridgman model predicts some temperature dependence and the Arima potential models underpredict. The MD predicted ZrO_2 thermal conductivity is larger compared to the Bridgman model. The Arima models overpredict. The electronic contribution to thermal conductivity should be considered in the comparison with the experiments and this is done below.

Fig. 9(b) compares MD predictions of k_f for ZrO_2 , using the three potential models (the Teter, CRG and Arima). The CRG models

predict larger k_f compared with Teter and Arima models.

The k_e is obtained from

$$k_e = L\sigma_0 \exp\left(-\frac{\Delta E_{e.g}}{2k_B T}\right), \quad (40)$$

same with Eq. (30). The bandgap ($\Delta E_{e.g}$) of molten UO_2 is 2.5 eV using an integral equation approach [3] and the bandgap for amorphous ZrO_2 is 4.7 eV measured by electron energy loss spectroscopy (EELS) [55]. The pre-exponential factor σ_0 is found from $k_e(T_m)$ using the average experimental $[k(T_m)]$ and $[k_f(T_m)]$ from the MD results

$$k_e(T_m) = k(T_m) - k_f(T_m). \quad (41)$$

Total thermal conductivity is with (k_e) from Eq. (40) and assuming it is constant above the melting temperature

$$k(T) = k_f + k_e(T), \quad (42)$$

For UO_2 , Fig. 10(a) shows the k_e and k as a function of

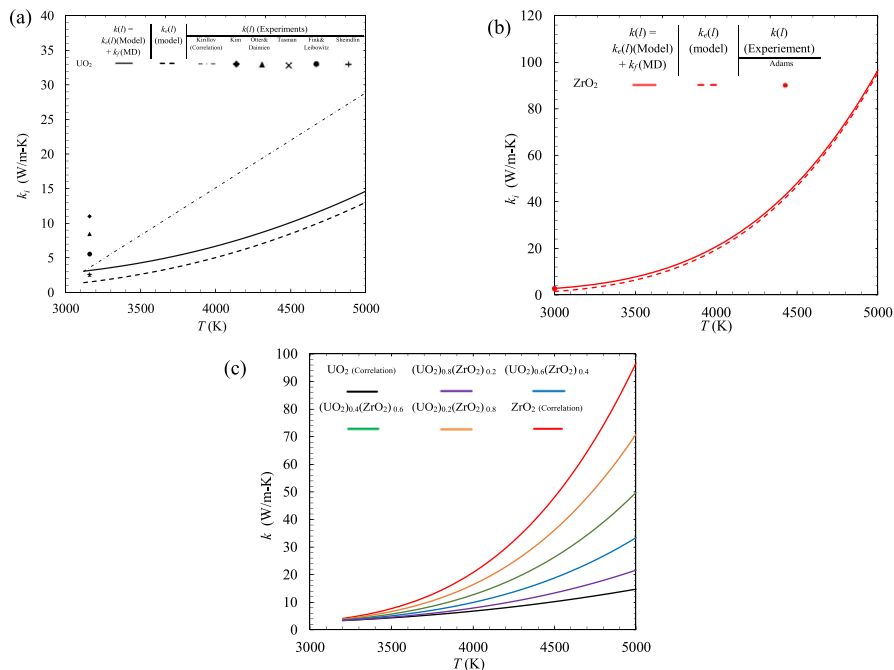


Fig. 10. (a) Variations of predicted liquid UO_2 electric and total thermal conductivity with temperature, and comparison with experiments. (b) Variations of predicted liquid ZrO_2 electric and total thermal conductivity with temperature, and comparison with experiments. (c) Variations of liquid UO_2 - ZrO_2 mixture (corium) thermal conductivity with temperature, and for several compositions.

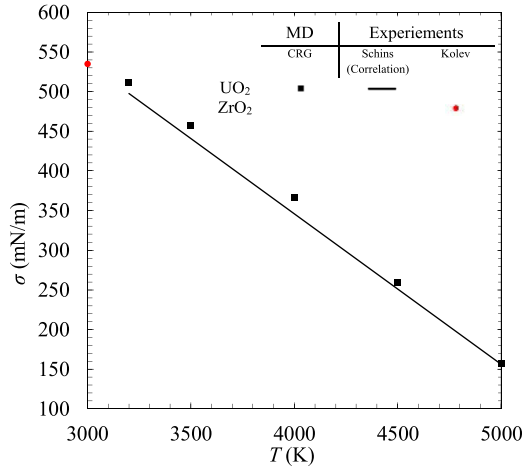


Fig. 11. Variations of MD predicted liquid UO₂ surface tension with temperature, and comparison with experiments (UO₂ and ZrO₂).

temperature and a fitting correlation

$$k(T) = 1.64 + 4.74 \times 10^{-2} T e^{-1.45 \times 10^4 / T}, \quad (43)$$

First term is the averaged k_f from the CRG potential. This correlation is compared with experiments [56–60] at melting temperature and correlation employed in the MATPRO code [61].

$$k(T) = 3.05 + 0.01375(T - 3120) \quad (\text{W/m-K}). \quad (44)$$

Compared to this extrapolate empirical correlation, our correlation based on theoretical model is expected to be more accurate.

Fig. 10(b) shows the temperature dependence of k_e and k for ZrO₂ using the Teter models for k_f , and a fitting correlation

$$k(T) = 2.11 + 4.46 T e^{-2.75 \times 10^4 / T}. \quad (45)$$

The predicted temperature dependent k_f for corium at several compositions are shown in Fig. 10(c), using Eq. (31), from (UO₂)_{0.8}(ZrO₂)_{0.2} to (UO₂)_{0.2}(ZrO₂)_{0.8} and above 3200 K (melting point of UO₂).

3.7. Surface tension

The surface tension of liquid UO₂ is predicted by the MD

simulations and the temperature dependent results are shown in Fig. 11 and compared with experiments with good agreements. The experimental correlation [62] is

$$\sigma(T) = 513 - 0.19(T - 3120) \quad (\text{mN/m}). \quad (46)$$

However, for ZrO₂ the MD predictions of the surface tension using both potentials (the CRG and Teter) models do not appear reasonable. This may be due to the incorrect interfacial-region stress tensor distribution. It seems that both models of ZrO₂ do not provide accurate free surface description, contrary to the precise predictions of the bulk state. The measured ZrO₂ surface tension at melting temperature [42] is also shown in Fig. 11, and is very close to the results for UO₂. It is thus expected that ZrO₂ surface tension and its temperature dependence is close to that of UO₂.

4. Summary

The thermophysical properties (density, compressibility, heat capacity, viscosity, surface tension, and thermal conductivity) of liquid UO₂ and ZrO₂ and their corium mixture are predicted using classical molecular dynamics simulations, up to 5000 K. The liquid behavior is verified with the random motion of the constituent atoms and the pair-distribution functions, starting with the solid phase and raising the temperature to realize the liquid phase. The viscosity and thermal conductivity are calculated with the Green-Kubo autocorrelation decay formulae and compared with the predictive models of Andrade and Bridgman. For liquid UO₂, the CRG model gives satisfactory MD predictions. For liquid ZrO₂, the density is reliably predicted with the CRG potential model, while the compressibility and viscosity are more accurately predicted by the Teter model. For liquid ZrO₂, the CRG potential models overpredict the bulk modulus (inverse of compressibility) and viscosity compared to the Teter models. The liquid electronic thermal conductivity model based on intrinsic semiconductor behavior and the Wiedemann-Franz law predicts total thermal liquid conductivity in good agreement with the experimental. The surface tension for UO₂ is reasonably predicted compared to the experimental results, whereas the predicted ZrO₂ results by the CRG and the Teter models do not appear reasonable. Newly proposed temperature-dependent correlations for liquid UO₂ and ZrO₂ and corium density, compressibility, heat capacity, heat of fusion, viscosity, surface tension, and thermal conductivity are provided in Table 5.

Table 5 Temperature-dependent correlations and the activation energy for liquid the UO₂ and ZrO₂ and corium properties using the Gross et al. and Hirai formulae.

Property	UO ₂	ZrO ₂	Mixtures (x : mole fraction)
Density (g/cm ³)	$\rho(T) = 4.40 - 8.31 \times 10^{-4}(T - 3120)$ (Based on CRG potential models)	$\rho(T) = 7.56 - 2.86 \times 10^{-4}(T - 2988)$ (Based on CRG potential models)	$\rho(T) = \frac{x_{UO_2} M_{UO_2} + (1 - x_{UO_2}) M_{ZrO_2}}{x_{UO_2} M_{UO_2} / \rho_{UO_2} + (1 - x_{UO_2}) M_{ZrO_2} / \rho_{ZrO_2}}$
Heat capacity (J/kg-K)	$c_V(T) = 390 - 0.900 \times 10^{-4} T$ (Based on CRG potential models)	$c_V(T) = 940 - 3.36 \times 10^{-2} T$ (Based on CRG potential models)	$c_V(T) = \frac{x_{UO_2} M_{UO_2} c_{V,UO_2} + (1 - x_{UO_2}) M_{ZrO_2} c_{V,ZrO_2}}{M_{UO_2} x_{UO_2} + M_{ZrO_2} (1 - x_{UO_2})}$
Heat of Fusion (kJ/kg)	218 (Based on CRG potential models)	260 (Based on CRG potential models)	$\Delta h_{sl} = \frac{x_{UO_2} M_{UO_2} \Delta h_{sl,UO_2} + (1 - x_{UO_2}) M_{ZrO_2} \Delta h_{sl,ZrO_2}}{M_{UO_2} x_{UO_2} + M_{ZrO_2} (1 - x_{UO_2})}$
Compressibility (1/MPa × 10 ⁻⁴)	$\kappa_f(T) = 0.124 - 6.60 \times 10^{-5} T + 4.33 \times 10^{-8} T^2$ (Based on CRG potential models)	$\kappa_f(T) = 1.51 - 7.97 \times 10^{-4} T + 1.38 \times 10^{-7} T^2$ (Based on Teter potential models)	$\kappa_f(T) = \frac{x_{UO_2} \kappa_{f,UO_2} M_{UO_2} / \rho_{UO_2} + (1 - x_{UO_2}) \kappa_{f,ZrO_2} M_{ZrO_2} / \rho_{ZrO_2}}{x_{UO_2} M_{UO_2} / \rho_{UO_2} + (1 - x_{UO_2}) M_{ZrO_2} / \rho_{ZrO_2}}$
Viscosity (mPa-s)	$\mu(T) = 0.520 e^{8.26 \times 10^3 / T}$ (Based on CRG potential models)	$\mu(T) = 0.320 e^{8.79 \times 10^3 / T}$ (Based on Teter potential models)	$\ln \mu(T) = x_{UO_2} \ln \mu_{UO_2}(T) + (1 - x_{UO_2}) \ln \mu_{ZrO_2}(T)$
Thermal conductivity $k(l) = k_e(l)$ (Model) + k_f (MD) (W/m-K)	$k(T) = 1.64 + 4.74 \times 10^{-2} T e^{-1.45 \times 10^4 / T}$ (Based on CRG potential models and experiment)	$k(T) = 2.11 + 4.46 T e^{-2.75 \times 10^4 / T}$ (Based on Teter potential models and experiment)	$k(T) = x_{UO_2} k_{UO_2} + x_{ZrO_2} k_{ZrO_2} - 0.72 x_{UO_2} (1 - x_{UO_2}) k_{UO_2} - k_{ZrO_2} $

$$\begin{aligned} \rho(T) &= 8.86 - 9.28 \times 10^{-4}(T - 3120) & \rho(T) &= 5.98 - 8.87 \times 10^{-4}(T - 2988) \\ \mu(T) &= 0.351 e^{8.79 \times 10^3 / T} & \mu(T) &= 0.312 e^{8.26 \times 10^3 / T} \end{aligned}$$

Acknowledgement

M.K. is thankful for support from NSF program on Thermal Transport Processes (Award No. CBET1332807). This research was also supported by National Nuclear R&D Program through the National Research Foundation of Korea (NRF) funded by the Ministry of Science, ICT and Future Planning (2013M2B2A9A03051257) and Basic Science Research Program through NRF funded by the Ministry of Education (2015R1D1A1A01059621). Thanks to Dr. M.W.D Cooper in Los Alamos National Laboratory (LANL) for providing additional Zr-O interatomic potential models.

References

- [1] P. Piluso, J. Moneris, C. Journeau, G. Cognet, Viscosity measurements of ceramic oxides by aerodynamic levitation, *Int. J. Thermophys.* 23 (2002) 1229–1240, <http://dx.doi.org/10.1023/A:1019844304593>.
- [2] G. Hwang, M. Kaviany, K. Moriyama, H.S. Park, B. Hwang, FARO tests corium-melt cooling in water pool: Roles of melt superheat and sintering in sediment, *Nucl. Eng. Des.* 305 (2016) 569–581, <http://dx.doi.org/10.1016/j.nucengdes.2016.05.039>.
- [3] D.A. MacInnes, D. Martin, A calculation of the electron band gap in molten UO₂, *J. Nucl. Mater.* 98 (1981) 241–246.
- [4] S.S. Abalin, V.G. Asmolov, V.D. Daragan, E.K. D'yakov, A.V. Merzlyakov, V.Y. Vishnevsky, Corium kinematic viscosity measurement, *Nucl. Eng. Des.* 200 (2000) 107–115, [http://dx.doi.org/10.1016/S0029-5493\(00\)00238-7](http://dx.doi.org/10.1016/S0029-5493(00)00238-7).
- [5] D.A. MacInnes, D. Martin, A calculation of the electron band gap in molten UO₂, *J. Nucl. Mater.* 98 (1981) 241–246, [http://dx.doi.org/10.1016/0022-3115\(81\)90150-1](http://dx.doi.org/10.1016/0022-3115(81)90150-1).
- [6] S. Plimpton, Fast parallel algorithms for short-range molecular dynamics, *J. Comput. Phys.* 117 (1995) 1–19, <http://dx.doi.org/10.1006/jcph.1995.1039>.
- [7] V. Levitin, The tight-binding model and embedded-atom potentials, in: *Interat. Bond. Solids*, Wiley-VCH Verlag GmbH & Co. KGaA, New York, NY, 2013, pp. 157–174, <http://dx.doi.org/10.1002/9783527671557.ch11>.
- [8] M.S. Daw, S.M. Foiles, M.I. Baskes, The embedded-atom method: a review of theory and applications, *Mater. Sci. Rep.* 9 (1993) 251–310, [http://dx.doi.org/10.1016/0920-2307\(93\)90001-U](http://dx.doi.org/10.1016/0920-2307(93)90001-U).
- [9] M.W.D. Cooper, M.J.D. Rushton, R.W. Grimes, A many-body potential approach to modelling the thermomechanical properties of actinide oxides, *J. Phys. Condens. Matter* 26 (2014) 105401, <http://dx.doi.org/10.1088/0953-8984/26/10/105401>.
- [10] X.-Y. Liu, M.W.D. Cooper, K.J. McClellan, J.C. Lashley, D.D. Byler, C.R. Stanek, et al., Thermal transport in UO₂ with Defects and Fission Products by Molecular Dynamics Simulations, Los Alamos National Laboratory (LANL), 2015.
- [11] R.A. Buckingham, The classical equation of state of gaseous helium, neon and argon, *Proc. R. Soc. Lond. A Math. Phys. Eng. Sci.* 168 (1938) 264–283, <http://rspa.royalsocietypublishing.org/content/168/933/264.abstract>.
- [12] J. Du, R. Devanathan, L. Corrales, W. Weber, A. Cormack, Short- and medium-range structure of amorphous zircon from molecular dynamics simulations, *Phys. Rev. B* 74 (2006) 214204, <http://dx.doi.org/10.1103/PhysRevB.74.214204>.
- [13] C.-S. Zha, H. Mao, R.J. Hemley, Elasticity of MgO and a primary pressure scale to 55 GPa, *Proc. Natl. Acad. Sci.* 97 (2000) 13494–13499, <http://dx.doi.org/10.1073/pnas.240466697>.
- [14] P.M. Morse, Diatomic molecules according to the wave mechanics. II. Vibrational levels, *Phys. Rev.* 34 (1929) 57–64, <http://dx.doi.org/10.1103/PhysRev.34.57>.
- [15] G.J. Ackland, Comprehensive nuclear materials, in: *Compr. Nucl. Mater.*, Elsevier, Amsterdam, AE, 2012, pp. 267–291, <http://dx.doi.org/10.1016/B978-0-08-056033-5.00026-4>.
- [16] W.K. Kim, J.H. Shim, M. Kaviany, UO₂ bicrystal phonon grain-boundary resistance by molecular dynamics and predictive models, *Int. J. Heat. Mass Transf.* 100 (2016) 243–249, <http://dx.doi.org/10.1016/j.jheatmasstransfer.2016.04.071>.
- [17] J.J.P. Stewart, Mopac2009, Stewart computational chemistry, Colorado springs, co, USA, <http://OpenMOPACnet>, 2008.
- [18] D. Wolf, Reconstruction of NaCl surfaces from a dipolar solution to the Madelung problem, *Phys. Rev. Lett.* 68 (1992) 3315–3318, <http://dx.doi.org/10.1103/PhysRevLett.68.3315>.
- [19] D. Wolf, P. Keblinski, S.R. Phillpot, J. Eggebrecht, Exact method for the simulation of Coulombic systems by spherically truncated, pairwise r⁻¹ summation, *J. Chem. Phys.* 110 (1999) 8254–8282, <http://dx.doi.org/10.1063/1.478738>.
- [20] P.P. Ewald, Die Berechnung optischer und elektrostatischer Gitterpotentiale, *Ann. Phys.* 369 (1921) 253–287, <http://dx.doi.org/10.1002/andp.19213690304>.
- [21] R.W. Hockney, J.W. Eastwood, *Computer Simulation Using Particles*, Adam Hilger, New York, 1989. There Is No Corresp. Rec. This Ref. (n.d.).
- [22] E.L. Pollock, J. Glosli, Comments on P3M, FMM, and the Ewald method for large periodic Coulombic systems, *Comput. Phys. Commun.* 95 (1996) 93–110, [http://dx.doi.org/10.1016/0010-4655\(96\)00043-4](http://dx.doi.org/10.1016/0010-4655(96)00043-4).
- [23] W.G. Hoover, Canonical dynamics: equilibrium phase-space distributions, *Phys. Rev. A* 31 (1985) 1695–1697, <http://link.aps.org/doi/10.1103/PhysRevA.31.1695>.
- [24] S. Nosé, A unified formulation of the constant temperature molecular dynamics methods, *J. Chem. Phys.* 81 (1984).
- [25] M. Parrinello, A. Rahman, Polymorphic transitions in single crystals: a new molecular dynamics method, *J. Appl. Phys.* 52 (1981).
- [26] A. Stukowski, Visualization and analysis of atomistic simulation data with OVITO—the Open Visualization Tool, *Model. Simul. Mater. Sci. Eng.* 18 (2009) 15012, <http://dx.doi.org/10.1088/0965-0393/18/1/015012>.
- [27] G. Arya, E.J. Maginn, H.C. Chang, Efficient viscosity estimation from molecular dynamics simulation via momentum impulse relaxation, *J. Chem. Phys.* 113 (2000) 2079–2087, <http://dx.doi.org/10.1063/1.482019>.
- [28] D.J. Evans, Peter T. Cummings, Nonequilibrium molecular dynamics properties and non newtonian fluid approaches to Transport rheology, *Ind. Eng. Chem. Res.* 31 (1992) 1237–1252, <http://dx.doi.org/10.1021/ie00005a001>.
- [29] a. J.H. McGaughey, M. Kaviany, Thermal conductivity decomposition and analysis using molecular dynamics simulations. Part I. Lennard-Jones argon, *Int. J. Heat. Mass Transf.* 47 (2004) 1783–1798, <http://dx.doi.org/10.1016/j.jheatmasstransfer.2003.11.002>.
- [30] M. Kaviany, *Heat Transfer Physics*, second ed., Cambridge University Press, New York, NY, 2014 <http://dx.doi.org/10.1017/CBO9780511754586>.
- [31] E.N. da C. Andrade, XLI. A theory of the viscosity of liquids.—Part I, London, Edinburgh, Dublin Philos. Mag. J. Sci. 17 (1934) 497–511, <http://dx.doi.org/10.1080/14786443409462409>.
- [32] F. Sudreau, G. Cognet, Corium viscosity modelling above liquidus temperature, *Nucl. Eng. Des.* 178 (1997) 269–277, [http://dx.doi.org/10.1016/S0029-5493\(97\)00137-4](http://dx.doi.org/10.1016/S0029-5493(97)00137-4).
- [33] S. Arrhenius, Über die innere Reibung verdünnter wässriger Lösungen, *Zeitschrift Für Phys. Chemie.* 1 (1887) 285–298.
- [34] S. Glasstone, H. Eyring, K.J. Laidler, *The Theory of Rate Processes*, McGraw-Hill, 1941.
- [35] S. Nazare, G. Ondracek, B. Schulz, *Properties of Light Water Reactor Core Melts*, 1976.
- [36] A.V. Grosse, The empirical relationship between the activation of energy viscosity of liquid metals and their melting points, *J. Inorg. Nucl. Chem.* 25 (1963) 317–318, [http://dx.doi.org/10.1016/0022-1902\(63\)80065-2](http://dx.doi.org/10.1016/0022-1902(63)80065-2).
- [37] M. Hirai, Estimation of viscosities of liquid alloys, *ISIJ Int.* 33 (1993) 251–258, <http://dx.doi.org/10.2355/isijinternational.33.251>.
- [38] P.W. Bridgman, The thermal conductivity of liquids under pressure, *Proc. Am. Acad. Arts Sci.* 59 (1923) 141–169, <http://dx.doi.org/10.2307/20026073>.
- [39] P. Resa, L. Elvira, Compressibility of liquid mixtures assuming incompressible cores, *Chem. Phys. Lett.* 481 (2009) 198–203, <http://dx.doi.org/10.1016/j.cplett.2009.09.069>.
- [40] P.L. Kirillov, M.I. Terenteva, N.B. Denisina, *Thermophysical Properties of Materials for Nuclear Engineering*, 2007.
- [41] W. Breitling, The density and compressibility of liquid (U, Pu)–mixed oxide, *Nucl. Sci. Eng.* 217 (1990) 205–217.
- [42] N.I. Kolev, *Multiphase Flow Dynamics 5: Nuclear Thermal Hydraulics*, Springer Berlin Heidelberg, 2011. <https://books.google.co.kr/books?id=eQFMHfNsAaEC>.
- [43] H. Kim, M.H. Kim, M. Kaviany, Lattice thermal conductivity of UO₂ using ab initio and classical molecular dynamics, *J. Appl. Phys.* 115 (2014), <http://dx.doi.org/10.1063/1.4869669>.
- [44] L.P. Filippov, N.S. Novoselova, Thermal conductivity of Normal Liquid Solutions, *Vest. Mask. Gos. Univ. Ser. Fiz.* (1955) 37–40.
- [45] G.N. Dul'nev, Yu. P. Zarichnyak, Inzhenerno-Fizicheskii, G.N. Dul'nev, Y.P. Zarichnyak, Thermal conductivity of liquid mixtures, *J. Eng. Phys.* 11 (1966) 400–402, <http://dx.doi.org/10.1007/BF00829337>.
- [46] J.C. Kirkwood, F.P. Buff, The statistical mechanical theory of surface tension, *J. Chem. Phys.* 17 (1949) 338–343.
- [47] S.A. Nelson, I.S.E. Carmichael, Partial molar volumes of oxide components in silicate liquids, *Contrib. Mineral. Petrol.* 71 (1979) 117–124, <http://dx.doi.org/10.1007/BF00375427>.
- [48] C. Ronchi, M. Sheindlin, M. Musella, G.J. Hyland, Thermal conductivity of uranium dioxide up to 2900 K from simultaneous measurement of the heat capacity and thermal diffusivity, *J. Appl. Phys.* 85 (1999) 776–789, <http://dx.doi.org/10.1063/1.369159>.
- [49] M.H. Rand, R.J. Ackermann, F. Gronvold, F.L. Oetting, A. Pattoret, The thermodynamic properties of the urania phase, *Rev. Int. Des. Hautes Temp. Des. Refract* 15 (1978) 355–365.
- [50] E.A. Fischer, A new evaluation of the urania equation of state based on recent vapor pressure measurements, *Nucl. Sci. Eng.* 101 (1989) 97–116.
- [51] S.G. Popov, J.J. Carbajo, G.L. Yoder, Thermophysical properties of MOX and UO₂ fuels including the effects of irradiation, *ORNL* 27 (2000) 0–4.
- [52] D.L. Hargman, G.A. Reymann, MATPRO-Version 11: A handbook of materials properties for use in the analysis of light water reactor fuel rod behavior, Idaho National Engineering Lab, Idaho Falls (USA), 1979.
- [53] P.L. Kirillov, *Thermo Physical Properties of Materials for Nuclear Engineering*, Inst. Heat. Mass Transf. Nucl. Power Plants, Obninsk, 2006.
- [54] T. Arima, Melting point and thermal conductivity of UO₂-ZrO₂ solid solution: molecular dynamics simulation, *J. Comput. Chem. Jpn.* 14 (2015) 97–104, <http://dx.doi.org/10.2477/jccj.2015-0007>.
- [55] V. Gritsenko, D. Gritsenko, S. Shaimeev, V. Aliev, K. Nasyrov, S. Erenburg, et al.,

- Atomic and electronic structures of amorphous ZrO₂ and HfO₂ films, *Microelectron. Eng.* 81 (2005) 524–529, <http://dx.doi.org/10.1016/j.mee.2005.03.056>.
- [56] C.S. Kim, R.A. Blomquist, J. Haley, J. Fischer, M.G. Chasanov, L. Leibowitz, Measurement of Thermal Diffusivity of Molten UO₂, Argonne National Lab, 1977.
- [57] C. Otter, D. Damien, Mesure de la diffusivité thermique de UO₂ fondu, *High Temp. High. Press.* 16 (1984) 1–6.
- [58] H.A. Tasman, D. Pel, J. Richter, H.-E. Schmidt, Measurement of the thermal conductivity of liquid UO₂, *High. Temp. High. Press.* 15 (1983) 419–431.
- [59] J.K. Fink, L. Leibowitz, Analysis of Measurements of the Thermal Conductivity of Liquid Urania, Argonne National Lab., IL (USA), 1984.
- [60] M. Sheindlin, D. Staicu, C. Ronchi, L. Game-Arnaud, B. Remy, A. Degiovanni, Experimental determination of the thermal conductivity of liquid UO₂ near the melting point, *J. Appl. Phys.* 101 (2007) 0–9, <http://dx.doi.org/10.1063/1.2721091>.
- [61] P.E. MacDonald, L.B. Thompson, MATPRO: a Handbook of Materials Properties for Use in the Analysis of Light Water Reactor Fuel Rod Behavior, 1976 (Accessed June 22, 2016), http://inis.iaea.org/Search/search.aspx?orig_q=RN:7269069.
- [62] H. Schins, On the surface tension of liquid UO₂, *J. Nucl. Mater* 78 (1978) 215–216.